Article

Catalytic ozone decomposition and adsorptive VOCs removal in bimetallic metal-organic frameworks

Chen Dong[1,3], Jia-Jia Yang[2,3], Lin-Hua Xie [iD][1] ✉, Ganglong Cui [iD][2] ✉, Wei-Hai Fang [iD][2] & Jian-Rong Li [iD][1] ✉

Atmospheric ozone has long been a threat to human health, however, rational design of high-performance O_3-decomposition catalysts remains challenging. Herein, we demonstrate the great potential of a series of isomorphous bimetallic MOFs denoted as PCN-250(Fe_2M) (M = Co^{2+}, Ni^{2+}, Mn^{2+}) in catalytic O_3 decomposition. Particularly, PCN-250(Fe_2Co) showed 100% O_3 removal efficiency for a continuous air flow containing 1 ppm O_3 over a wide humidity range (0 – 80% RH) at room temperature. Mechanism studies suggested that the high catalytic performance originated from the introduction of open Co(II) sites as well as its porous structure. Additionally, at low pressures around 10 Pa, PCN-250(Fe_2Co) exhibited high adsorption capacities (89 – 241 mg g^{-1}) for most VOCs, which are not only a class of hazardous air pollutants but also the precursor of O_3. This work opens up a new avenue to develop advanced air purification materials for O_3 and VOCs removal in one.

Ground-level ozone (O_3) has long been a threat to human health, especially in urban area[1–3]. Outdoor O_3 is mostly generated from the photochemical reactions between nitrogen dioxides and volatile organic compounds (VOCs) in the air under sunlight[4,5]. Indoor O_3 is from indoor-outdoor air exchange as well as some emission sources include photocopiers, laser printers, ultraviolet lamps, and O_3 disinfectors[6–8]. Although being highly reactive as a very strong oxidizing agent, O_3 itself is relatively stable and nearly does not spontaneously decompose to oxygen (O_2) at the concentrations (ppb level) that are typically encountered in ambient air[6]. Plenty of studies have demonstrated the potential risk of respiratory and cardiovascular mortality for the human body after long-term exposure to the air with a trace of O_3[9,10]. The World Health Organization has recommended that the 8-h daily maximum O_3 concentration in ambient air exceeding 100 µg m^{-3} (~51 ppb) poses health risks[11]. However, the occurrence of severe warm-season O_3 pollution has become more frequent in the past few years for both developing and developed countries[7,12]. For example, field observations and satellite retrievals reveal that the

observed hourly maximum O_3 concentrations in China frequently exceeded 150 ppb (severe O_3 pollution)[13,14]. The study to reduce O_3 pollution is thus in high demand for the protection of the environment and human health.

The existing approaches to remove O_3 from ambient air are typically based on activated carbon adsorption, chemical absorption, and catalytic decomposition methods[15–18]. Among them, catalytic decomposition of O_3 into O_2 at low temperatures is promising because of its ease in operation, high efficiency, good persistence, and environmental friendliness[19,20]. Over the past decades, significant advances have been made in catalytic O_3 degradation using transition metal (Mn[21], Fe[22], Co[23], Ni[24], and Cu[25]) oxides mostly. As a class of newly emerged materials, metal-organic frameworks (MOFs) have attracted great interest in various catalytic reactions because of their tunable structure and diverse functionality, including O_3 catalytic decomposition[26–31]. In addition, compared with transition metal oxides, MOFs can have highly porous structures, thus may offer extra catalytically active sites on interior pore surface, and even serve as advanced multifunctional materials to

[1]Beijing Key Laboratory for Green Catalysis and Separation, and Department of Environmental Chemical Engineering, Beijing University of Technology, 100124 Beijing, China. [2]Key Laboratory of Theoretical and Computational Photochemistry, Ministry of Education, College of Chemistry, Beijing Normal University, 100875 Beijing, China. [3]These authors contributed equally: Chen Dong, Jia-Jia Yang. ✉e-mail: xielinhua@bjut.edu.cn; ganglong.cui@bnu.edu.cn; jrli@bjut.edu.cn
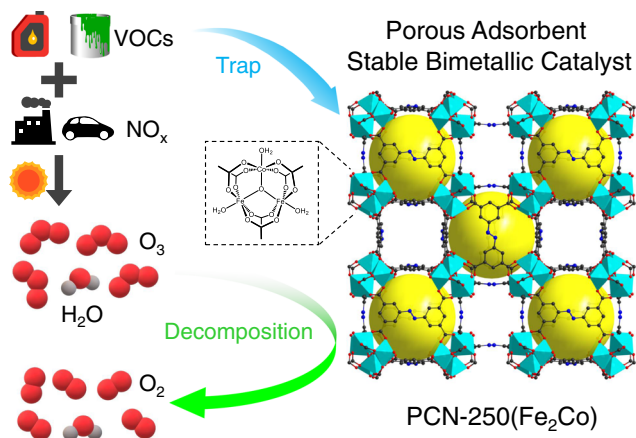
Fig. 1 | Schematic representation of the bimetallic MOF PCN-250(Fe$_2$Co) as a porous catalyst for both O$_3$ and VOCs removal. The O, C, N atoms, MO$_6$ units (M = Fe or Co) and cages in PCN-250(Fe$_2$Co) are represented by red, black, blue spheres, turquoise polyhedra, and large yellow spheres, respectively.

decompose O$_3$ and remove other airborne hazardous molecules by adsorption simultaneously[32–36]. Indeed, there exist kinds of air pollutants in some real application scenarios. For example, non-thermal plasma (NTP) is a highly efficient technology for VOCs removal and has been widely used for the past two decades, but the exhausted gases of NTP reactors usually contain the by-product O$_3$ as well as some incompletely decomposed VOCs[37]. It is thus highly desirable but still challenging to develop highly efficient, porous, and stable MOFs as such multifunctional air filtering materials.

The catalytically active sites in MOFs are commonly metal centers, and most reported MOFs are monometallic. Generating multimetallic building units in MOFs has been recently proposed as an effective strategy to regulate their catalytic properties[38,39]. Exploring multimetallic MOFs for catalytic O$_3$ decomposition would be intriguing. The MOF PCN-250(Fe$_3$)[40] (also known as MIL-127(Fe)[41]) constructed from Fe$_3$-μ_3-oxo clusters and ABTC^{4-} ligands (H$_4$ABTC = 3,3',5,5'-azobenzenetetracarboxylic acid) is a preferred platform for such a study because one Fe(III) ion of the Fe$_3$-μ_3-oxo cluster can be readily substituted by a common divalent transition metal ion, e.g., Co(II), Ni(II), and Mn(II), and this MOF can be facilely prepared with high stability and high porosity. Herein, we demonstrate the great potential of these bimetallic MOFs PCN-250(Fe$_2$M) (M = Co^{2+}, Ni^{2+}, Mn^{2+}) for catalytic O$_3$ removal from ambient air, especially PCN-250(Fe$_2$Co). It is also found that PCN-250(Fe$_2$Co) shows a high capacity in the adsorptive removal of volatile organic compounds (VOCs) (Fig. 1), which are not only a class of hazardous air pollutants but also the precursor of O$_3$. It is an attribution not available for most of the other O$_3$-decomposition catalysts. This study suggests the great potential of MOF-based materials for O$_3$ pollution control and also offers insights into the design of new air purification materials.

Results
Synthesis and characterization
Three bimetallic MOFs PCN-250(Fe$_2$M) (M = Co^{2+}, Ni^{2+}, Mn^{2+}), as well as their monometallic counterpart PCN-250(Fe$_3$), were prepared by the reported method with some modifications to evaluate their performances on catalytic O$_3$ decomposition. PXRD patterns of the four samples all showed strong peaks and well matched the simulated PXRD pattern of PCN-250(Fe$_3$) (Supplementary Fig. 2), confirming that their structures are isomorphous and the samples are in high crystallinity and purity. N$_2$ sorption isotherms of the four MOFs recorded at 77 K were all classic type-I isotherms for microporous materials (Supplementary Figs. 3–6). The pore volumes and BET surface areas of PCN-250(Fe$_3$), PCN-250(Fe$_2$Co), PCN-250(Fe$_2$Ni), and PCN-250(Fe$_2$Mn) were

estimated to be 0.52, 0.59, 0.58, and 0.57 cm^3 g^{-1}, and 1408, 1478, 1465, and 1443 m^2 g^{-1} with a pore size distribution of 7.0–11.5 Å, respectively. Thermal gravimetric analysis (TGA) curves suggested that the four MOFs thermally decomposed at about 400 °C (Supplementary Fig. 7). X-ray photoelectron spectra (XPS) analyses confirmed the presence of only Fe(III) ions in PCN-250(Fe$_3$) and the presence of both divalent metal ions (Co^{2+}, Ni^{2+}, or Mn^{2+}) and trivalent Fe^{3+} ions in the three bimetallic MOFs (Supplementary Figs. 8–11), which was further confirmed by the results of inductively coupled plasma-atomic emission spectroscopy (ICP-AES) measurements for digested samples of the MOFs (Supplementary Table 7) and EDS mapping images for the PCN-250 crystals (Supplementary Fig. 12).

Catalytic activity for O$_3$ decomposition
Catalytic O$_3$ decomposition experiments were conducted with continuous-flow fixed-bed reactors of the tested materials (30 mg) at ambient temperature and pressure, and the inlet gas flow rate was 1 L min^{-1} (see supplementary information for details). Considering the concentration of O$_3$ in ambient air is normally in the range of tens to hundreds of ppb, the O$_3$ concentration of inlet gas was set to be 1 ppm (balance air). For dry inlet gas (zero air), the three bimetallic MOFs PCN-250(Fe$_2$Co), PCN-250(Fe$_2$Mn), and PCN-250(Fe$_2$Ni) completely removed the O$_3$ of inlet gas during 12 h of continuous testing, while the O$_3$ removal efficiency of PCN-250(Fe$_3$) was around 85% (Fig. 2a). When the humidity of the inlet gas increased to RH = 40% (relative humidity at room temperature), the performances of the four MOFs became more different (Fig. 2b). For PCN-250(Fe$_2$Mn), PCN-250(Fe$_2$Ni), and PCN-250(Fe$_3$), the initial O$_3$ removal efficiencies were 97%, 89%, and 78%, which gradually decreased in the first 2 h and stabilized at 92%, 85%, and 75% in the following 10 h, respectively. In contrast, PCN-250(Fe$_2$Co) still retained 100% O$_3$ removal efficiency throughout the test. These results revealed that the three bimetallic MOFs were more catalytically active than PCN-250(Fe$_3$) for the decomposition reaction of O$_3$, and the O$_3$ removal performances of PCN-250(Fe$_3$), PCN-250(Fe$_2$Ni), and PCN-250(Fe$_2$Mn) could be affected by the humidity of inlet gas. It is common that the O$_3$ decomposition performances of catalysts reduce under more humid conditions[21,22]. Notably, PCN-250(Fe$_2$Co) showed 100% O$_3$ removal efficiency under both dry and humid conditions, suggesting that it has the highest catalytic activity among the four MOFs.

For comparison, the O$_3$ removal performances of some representative materials were also evaluated under the same experimental conditions, including two MOFs previously reported to show high O$_3$ degradation activities, ZZU-281[31] and MIL-100(Fe)[30], three metal oxides, α-Fe$_2$O$_3$[15], Co$_3$O$_4$[22], and CoFe$_2$O$_4$[42], and a common adsorbent widely used in air purification, activated charcoal[43]. The structure, purity, and/or porosity of these reference materials were confirmed (Supplementary Figs. 16–22). As shown in Fig. 2c, d, the O$_3$ removal efficiency of Co$_3$O$_4$ was around 45% under both dry and humid conditions. The O$_3$ removal efficiencies of MIL-100(Fe) and α-Fe$_2$O$_3$ were close after 12 h continuous testing, being ~75% and 65% under dry and humid conditions, respectively. The O$_3$ removal efficiencies of activated charcoal and CoFe$_2$O$_4$ decreased from 91 to 70% and 100 to 40% within 12 h under humid conditions, respectively, although their O$_3$ removal efficiencies under dry conditions were >99% throughout the test. The continuous decline in O$_3$ removal performance of activated charcoal under both dry and humid conditions may be attributed to the gradual consumption of O$_3$ reactive sites (e.g., hydroxyl groups) on the sample surface[44]. In addition, it is noteworthy that the O$_3$ removal performance of the bimetallic oxide CoFe$_2$O$_4$ is quite different from that of the physical mixture of Co$_3$O$_4$ and α-Fe$_2$O$_3$ (Supplementary Fig. 23). Among these reference materials, only ZZU-281 completely removed O$_3$ in inlet gases under both dry and humid conditions as PCN-250(Fe$_2$Co) did. To further validate the experimental results, commercial O$_3$ test strips were used to detect the O$_3$ concentration of
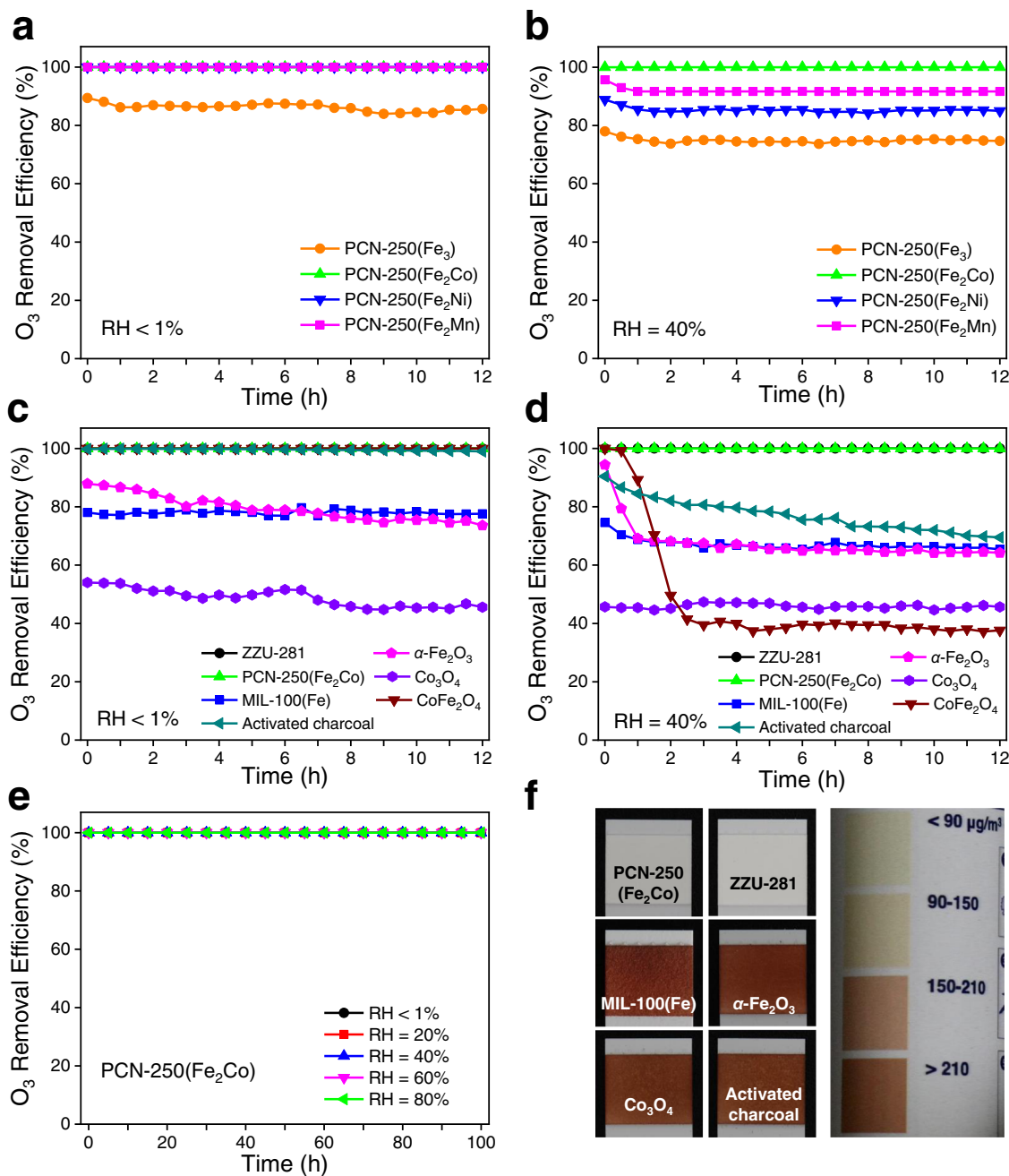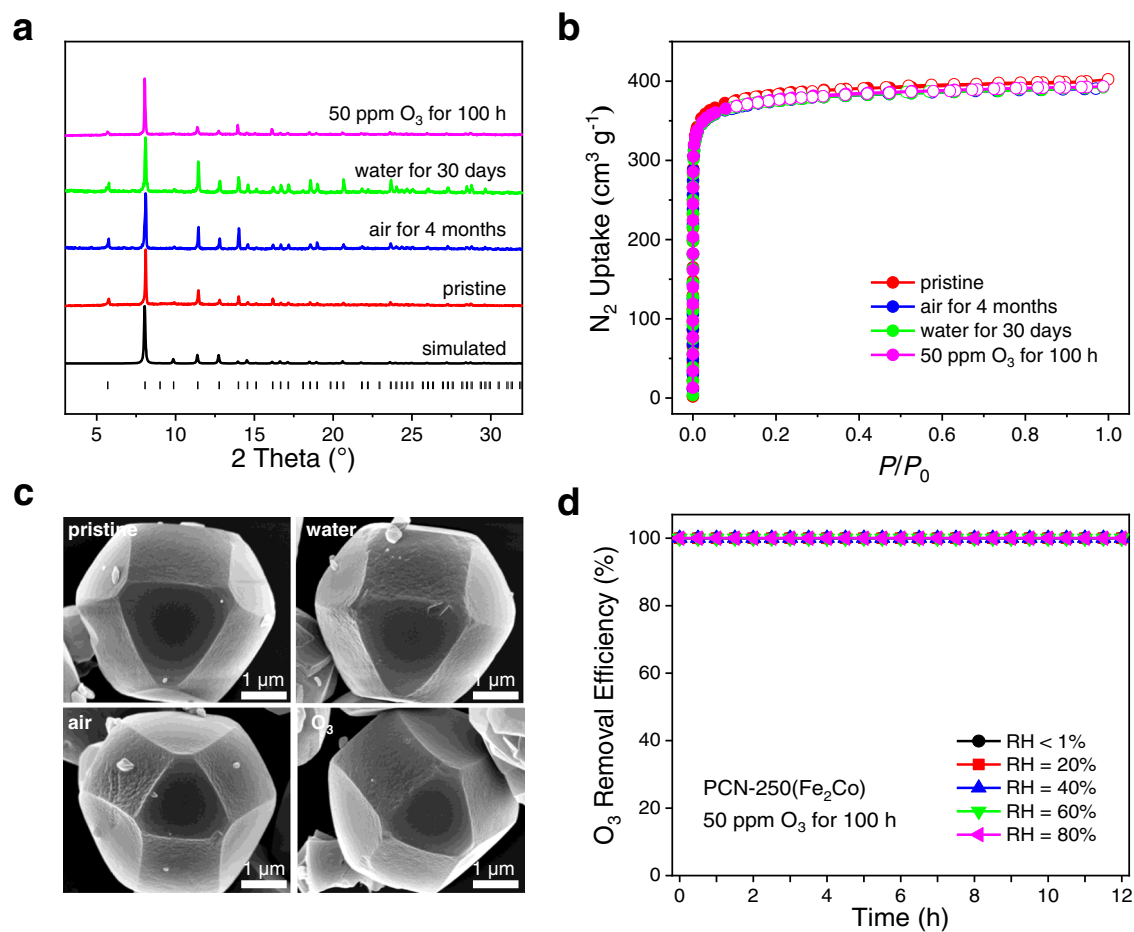
Fig. 2 | The O₃ removal efficiencies for PCN-250 and other reference materials.
a RH < 1% (zero air) and **b** RH = 40% for the PCN-250 samples. **c** RH < 1% (zero air) and **d** RH = 40% for PCN-250(Fe₂Co), ZZU-281, MIL-100(Fe), α-Fe₂O₃, Co₃O₄, CoFe₂O₄, and activated charcoal. **e** Varied RHs for PCN-250(Fe₂Co). Other conditions for all the above tests: 0.03 g catalyst diluted with 0.2 g quartz sand, concentration of O₃ = 1 ppm, flow rate = 1 L min⁻¹, room temperature. **f** O₃ test strips used in the tests under humid condition (RH = 40%) and the color scale.

outlet gases that respectively passed through the materials under humid conditions (RH = 40%). As the O₃ concentration of test gas increases, the strips change from white (ozone-free) to light-yellow (O₃ concentrations around 90 μg m⁻³) and then to brown (O₃ concentrations higher than 210 μg m⁻³) (Fig. 2f, right). The observed colors of the strips applied to the materials confirmed their different O₃ removal efficiencies (Fig. 2f, left).

The O₃ removal performances of PCN-250(Fe₂Co) under various humidity and longer testing duration were also investigated. As shown in Fig. 2e, PCN-250(Fe₂Co) kept 100% O₃ removal efficiency within 100 h of continuous testing when the RH of inlet gas varied from <1% (dry zero air) to 80%. We further explored the effects of the weight amount of PCN-250(Fe₂Co) and the O₃ concentration of inlet gas on

the O₃ removal efficiency of PCN-250(Fe₂Co). Control experiments were carried out after the weight amount of PCN-250(Fe₂Co) was reduced from 30 mg to 15 mg or the O₃ concentration of inlet gas was increased from 1 ppm to 50 ppm. For dry inlet gas, the O₃ removal efficiency of PCN-250(Fe₂Co) maintained 100% in both cases; for humid inlet gas (RH = 40% at room temperature), the O₃ removal efficiency of PCN-250(Fe₂Co) reduced to around 65% and 35%, respectively (Supplementary Fig. 24). These results revealed that the catalytic O₃ degradation capacity of PCN-250(Fe₂Co) under dry condition was higher than that under humid condition, as also observed for the other three PCN-250 MOFs. The different O₃ removal efficiencies of PCN-250(Fe₂Co) for dry and humid gases were also confirmed by cycling tests where the humidity of the gas flow was

Fig. 3 | Stability tests for PCN-250(Fe₂Co). a PXRD patterns, **b** N₂ sorption isotherms, and **c** SEM images of the pristine and stability-tested PCN-250(Fe₂Co) samples. **d** O₃ removal efficiencies for PCN-250(Fe₂Co) after 50 ppm O₃ treatment.

Test conditions: 0.03 g catalyst diluted with 0.2 g quartz sand, concentration of O_3 = 1 ppm, flow rate = 1 L min⁻¹, room temperature.

alternately changed (Supplementary Fig. 25). Under the dry condition, the O₃ removal efficiency of PCN-250(Fe₂Co) was 100% even if the O₃ concentration of inlet gas was further increased to 200 ppm, even much higher than that of ZZU-281 under the same condition (Supplementary Fig. 26). The different O₃ degradation performance of PCN-250(Fe₂Co) under dry and humid conditions may be originated from two aspects. On the one hand, PCN-250(Fe₂Co) is moderately hydrophilic as indicated by its water vapor adsorption isotherm at 298 K, where the water uptake gradually increases to 27 mmol g⁻¹ at 0.6 P/P_0 and keeps nearly unchanged at higher pressures (Supplementary Fig. 27). The water contact angle of the powder sample of PCN-250(Fe₂Co) is about 11° (Supplementary Fig. 28), indicating that the crystal surface is also moderately hydrophilic. Under humid conditions, adsorbed water molecules would partially or even fully block the pores of PCN-250(Fe₂Co), reducing the amount of accessible catalytically active sites on the interior pore surface to contact with O₃ molecules. On the other hand, water molecules may participate in the catalytic O₃ decomposition reaction, and the resulting new reaction pathway requires higher activation energy. Indeed, it was found that the O₃ removal efficiency of PCN-250(Fe₂Co) under humid conditions could be largely improved by generally heating the reactor to 45 °C (Supplementary Fig. 29).

For the practical application of O₃ removal, the long-term stability of catalysts under real working conditions is highly important[45]. The stability issue is especially outstanding for MOF-type catalysts since a large number of MOFs have been proven unstable even in ambient air[46]. In the last few years, a few MOFs showing high stability in water,

even under harsh acidic or basic conditions, have been reported, whereas there are very little knowledge about the stability of MOFs when exposed to O₃-containing air[47–52]. The high hydrolytic stability of PCN-250 MOFs has been well documented in the literature[53]. The long-term hydrolytic stability of PCN-250(Fe₂Co) was further tested by soaking it in water at room temperature for 30 days and by exposing it to ambient air for 4 months. PXRD and N₂ sorption measurement results revealed that the PCN-250(Fe₂Co) samples well maintained their high crystallinity and porosity after these treatments (Fig. 3a, b). No obvious change was observed by SEM for the crystal morphology and surface of PCN-250(Fe₂Co) (Fig. 3c).

As a strong oxidizing agent, O₃ is highly reactive to many substances, e.g., destroying organic compounds containing carbon-carbon double bonds, carbon-carbon triple bonds, and porphyrin rings[54–56]. Therefore, besides hydrolytic stability, the materials used for O₃ removal should also be able to resist long-term O₃ attack. The tolerance of PCN-250(Fe₂Co) to airborne O₃ (1 ppm) was indicated by its stable O₃ removal efficiency in the 100 h tests discussed above (Fig. 2e). Its tolerance was further evaluated by exposing it to a continuous flow (flow rate: 0.5 L min⁻¹) of dry or humid air (RH = 40% at room temperature) containing 50 ppm O₃ for 100 h (50 h for wet gas, and 50 h for dry gas) at room temperature. The comparison of PXRD patterns, N₂ adsorption isotherms, and SEM images for the O₃ treated and pristine PCN-250(Fe₂Co) samples suggested a high tolerance of PCN-250(Fe₂Co) to O₃ containing ambient air (Fig. 3a–c). Further experiments indicated that the four PCN-250 samples all are highly tolerant of O₃ (Supplementary Figs. 2–11). Moreover, the 50 ppm O₃

treated PCN-250(Fe$_2$Co) still showed 100% O$_3$ removal efficiency to dry or humid air (RH = 40% at room temperature) containing 1 ppm O$_3$ as the pristine sample did (Fig. 3d). Unexpectedly, it was found that some MOFs commonly regarded to be highly stable easily degraded after exposure to O$_3$ containing ambient air, e.g., ZIF-8, ZIF-L, and MIL-101(Cr). After being exposed to the flow of humid air containing 1 ppm O$_3$ for 24 h, the sample of ZIF-8 changed from white powder to light-yellow viscous liquid and completely lost its initial crystalline structure (Supplementary Fig. 30). The change was faster (in 4 h) when the O$_3$ concentration was increased to 50 ppm. Similar results were also observed for ZIF-L, which is built from the same metal ions and organic ligands as ZIF-8 (Supplementary Fig. 31). Although being more tolerant of O$_3$ in humid air than the two ZIFs, MIL-101(Cr) also lost crystallinity and changed color after exposing to the flow of O$_3$ containing humid air for 24 h (Supplementary Fig. 32). Therefore, PCN-250(Fe$_2$Co) represents a rare and excellent catalyst for O$_3$ decomposition due to its high stability and activity.

O$_3$ decomposition mechanism

To explore the source of the high O$_3$ decomposition activity of PCN-250(Fe$_2$Co), O$_3$ removal tests were also conducted for its starting materials, namely, the H$_4$ABTC ligand and the [Fe$_2$Co(μ$_3$-O)(CH$_3$COO)$_6$] complex. As shown in Supplementary Fig. 33, the O$_3$ removal efficiency of H$_4$ABTC was nearly negligible, but the [Fe$_2$Co(μ$_3$-O)(CH$_3$COO)$_6$] complex could remove 60–90% O$_3$ in inlet gas under dry and humid conditions. These results indicated that the catalytic active sites of PCN-250(Fe$_2$Co) for O$_3$ decomposition were the metal centers of Fe$_2$Co-μ$_3$-oxo clusters which are bonding with labile water molecules. It is also revealed that assembling the starting materials into the highly open MOF structure was beneficial to achieve a higher O$_3$ removal efficiency due to the increase of accessible catalytic active sites exposed on the pore surface. Since the four PCN-250 MOFs are isomorphous and PCN-250(Fe$_2$Co) showed the highest O$_3$ removal efficiency, Co(II) center should be the most active catalytic site for O$_3$ decomposition among the four types of metal centers (Fe^{3+}, Co^{2+}, Ni^{2+}, and Mn^{2+}). In addition, the catalytic reaction mechanisms under humid and dry conditions should be different according to the experimental results. Density functional theory (DFT) calculations were carried out with a [Fe$_2$Co(μ$_3$-O)(PhCOO)$_6$] cluster model to reveal the O$_3$ decomposition mechanism at the Co(II) site of PCN-250(Fe$_2$Co) and the following reaction pathways were proposed (see supplementary information for details). Under the humid condition, as shown in Fig. 4a, c, the H atom of H$_2$O* adsorbed on the Co(II) atom first attacks O$_3$ along with the formation of $^\cdot$OOOH and **OH radicals (* indicates the atom bonded to the Co atom). Subsequently, the remaining H atom of **OH is transferred to $^\cdot$OOOH generating O$_2$, H$_2$O, and $^\cdot$O* (State 3 in Fig. 4a and INT1-2, S = 16 in Fig. 4c). Then, another O$_3$ molecule attacks $^\cdot$O* releasing two O$_2$ molecules. Afterward, the Co(II) atom becomes coordinatively unsaturated and prefers to coordinate with H$_2$O over O$_3$ under the humid condition due to the favorable adsorption energy of the former (22.4 vs. 9.0 kcal mol^{-1}). As a result, the initial state is regenerated, and the catalysis repeats. Throughout the entire catalytic process, the first H transfer is a rate-determining step with a barrier of 15.9 kcal mol^{-1} (TS1-1, S = 14 in Fig. 4c, and Supplementary Table 2).

Differently, under dry conditions, the reaction pathway essentially starts from the coordinatively unsaturated Co(II) center, which is generated by the reaction pathway under humid conditions (from State 1 to State 5 in Fig. 4a). O$_3$ first binds to the exposed Co(II) center and then the *O$_3$ splits into O$_2$ and $^\cdot$O* with a barrier of 9.4 kcal mol^{-1} (State 3 in Fig. 4b, TS2-1, S = 14 in Fig. 4d, and Supplementary Table 3). Afterward, another O$_3$ molecule attacks $^\cdot$O*, resulting in two O$_2$ molecules and a coordinatively unsaturated Co(II) center (State 1 in Fig. 4b, and PROD2, S = 14 in Fig. 4d). The barrier of the rate-determining step in the dry condition is estimated to be 9.4 kcal mol^{-1}. It is clear from the above computational results that the rate-determining step in both

humid and dry conditions is related to their first elementary reaction, namely the H transfer in the former and the O$_3$ decomposition in the latter. Importantly, the barrier of the rate-determining step is smaller in the dry condition than that in the humid condition (9.4 and 15.9 kcal mol^{-1}). In addition, it is an endergonic reaction step in the humid condition ($\Delta G = 11.8$ kcal mol^{-1}), while it becomes exergonic in the dry condition ($\Delta G = -5.4$ kcal mol^{-1}). Taken together, the dry condition is more favorable for the O$_3$ removal, which is consistent with the experimental results.

Moreover, we also calculated the rate-determining barriers of the O$_3$ decomposition at the Fe(III) site of [Fe$_2$Co(μ$_3$-O)(PhCOO)$_6$] and [Fe$_3$(μ$_3$-O)(PhCOO)$_6$]. In brief, both the Co(II) and Fe(III) sites share a similar catalytic mechanism. However, the Fe(III) site has larger barriers under either humid or dry conditions compared with the Co(II) site. Under humid and dry conditions, the barriers were calculated to be 21.5 and 14.8 kcal mol^{-1} for [Fe$_2$Co(μ$_3$-O)(PhCOO)$_6$] (Fig. 4e, f and Supplementary Table 5); while they were estimated to be 24.7 and 11.7 kcal mol^{-1} for [Fe$_3$(μ$_3$-O)(PhCOO)$_6$] (Supplementary Fig. 34 and Supplementary Table 6). The calculations clearly showed that the enhanced O$_3$ decomposition performance of PCN-250(Fe$_2$Co) originated from the introduction of open Co(II) sites.

VOCs adsorption of PCN-250(Fe$_2$Co)

Due to its high porosity and moderate pore size, PCN-250(Fe$_2$Co) is potentially capable of removing other pollutants in the air by adsorption besides O$_3$. VOCs are not only a class of hazardous air pollutants but also the precursor of O$_3$, the removal of VOCs from air is thus of high importance[35]. To evaluate its performance on VOCs removal, adsorption isotherms of PCN-250(Fe$_2$Co) were recorded at 25 °C for ten common VOCs, including methanol, acetone, two aliphatic hydrocarbons (n-hexane and cyclohexane) and six aromatic hydrocarbons (benzene, toluene, ethylbenzene, o-xylene, m-xylene, and p-xylene). Type-I adsorption isotherms were obtained for all the tested VOCs (Fig. 5a, b), showing an abrupt increase of uptakes at low vapor pressures below $P/P_0 = 0.002$ (Supplementary Fig. 35). At 0.01 kPa, the uptakes of methanol, acetone, n-hexane, cyclohexane, benzene, toluene, ethylbenzene, o-xylene, m-xylene, and p-xylene were 89, 177, 216, 123, 175, 241, 179, 114, 130, and 164 mg g^{-1} (Fig. 5c), respectively, corresponding to 18–75% of the maximum uptakes at 0.90–0.99 P/P_0 (174–652 mg g^{-1}). The high VOCs adsorption capacities of PCN-250(Fe$_2$Co) suggest that the MOF may serve as a general adsorbent to remove various VOCs even if the concentrations of VOCs are low. In practical application, the humidity of air can significantly affect the performance of adsorbents for VOCs removal. To check the effect of humidity on PCN-250(Fe$_2$Co), breakthrough experiments of dry and humid air flows containing 3000 ppm acetone vapor passing through a column of the MOF adsorbent (20 mg) were carried out at room temperature (see supplementary information for details). As shown in Fig. 5d, for dry gas, acetone started to penetrate the MOF column after about 190 s (160 min g^{-1}), corresponding to an acetone capture capacity of ca. 355 mg g^{-1} in the dynamic adsorption process, which is close to the theoretical uptake at 0.3 kPa (400 mg g^{-1}) from the static adsorption isotherm measurement. When the humidity of the gas mixture increased to RH = 40%, about 93% of the acetone capture capacity of PCN-250(Fe$_2$Co) retained, suggesting a good tolerance to the humidity of the MOF adsorbent for acetone vapor capture. Moreover, PXRD measurements revealed that PCN-250(Fe$_2$Co) also showed excellent stability toward the VOCs (Supplementary Fig. 36).

It is noteworthy that previously reported materials showing high performance on catalytic O$_3$ removal, such as the above-mentioned ZZU-281 and some advanced transition metal oxides[19,22,24], are of low porosity or nonporous and thus have limited capacity to adsorptively remove non-O$_3$ air pollutants like VOCs. In addition, compared with the most common and prevalent adsorbent for VOCs removal,
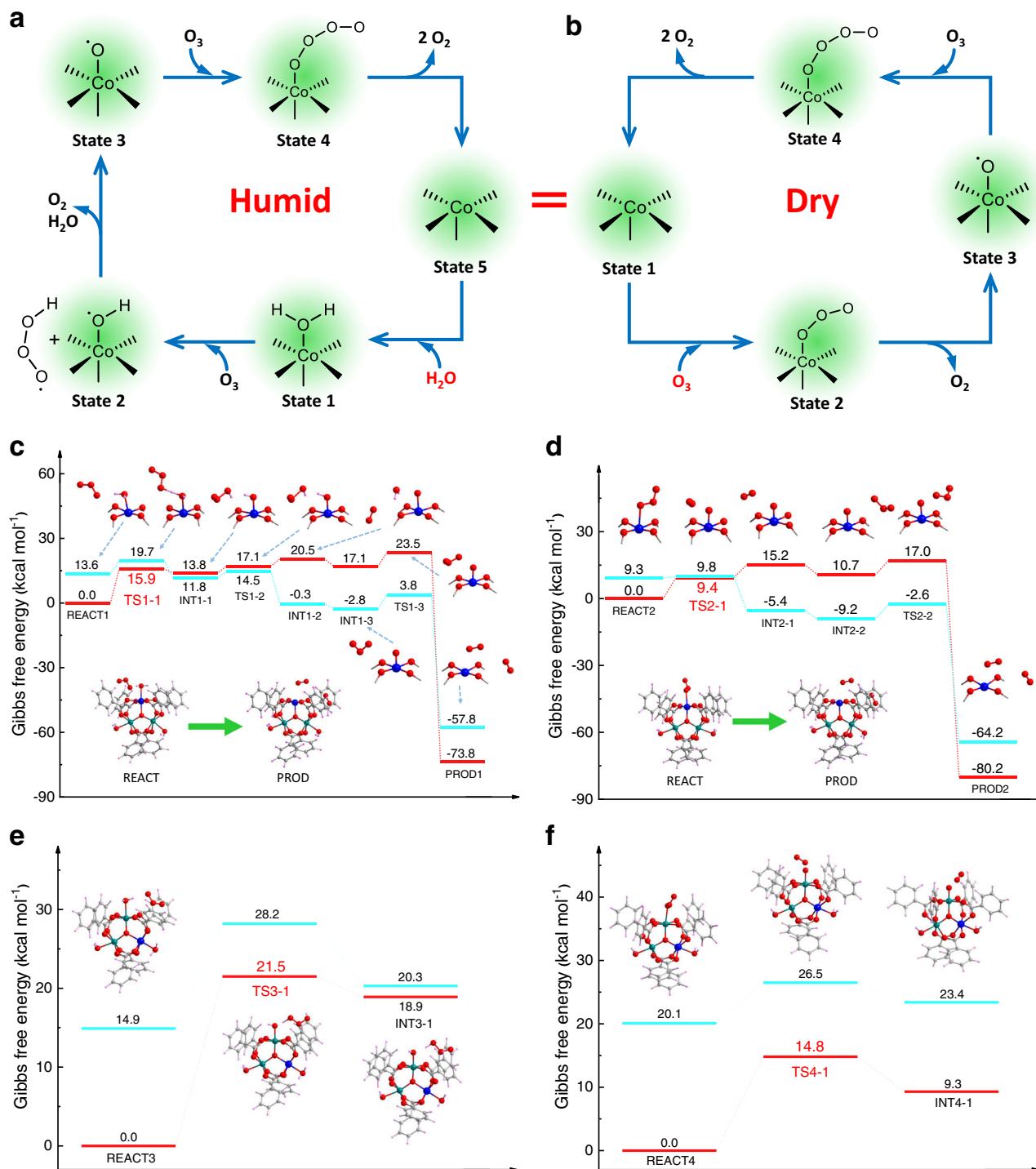
Fig. 4 | O₃ decomposition mechanism exploration. Proposed reaction pathways, energy profiles, and stationary-point structures along the calculated reaction pathways for the O₃ decomposition catalyzed at the Co(II) site of PCN-250(Fe₂Co) under both **a**, **c** humid and **b**, **d** dry conditions. Energy profiles and stationary-point structures along the calculated reaction pathways at the Fe(III) site of the PCN-250(Fe₂Co)-catalyzed O₃ decomposition under **e** humid and **f** dry conditions. Energy levels of the total spin state of S = 14 and S = 16 are shown in red and light blue, respectively. Color code: Co, blue; Fe, turquoise; C, gray; O, red; and H, pink.

activated charcoal, PCN-250(Fe₂Co), shows more stable performance and higher activity on catalytic O₃ removal. The high O₃ removal performance, high porosity, high stability, and facile preparation make PCN-250(Fe₂Co) a unique and promising multifunctional material for air purification.

Discussion

The great potential of isomorphous bimetallic MOFs PCN-250(Fe₂M) as high-performance porous catalysts for both O₃

degradation and VOCs removal is demonstrated. Particularly, PCN-250(Fe₂Co) showed 100% O₃ removal efficiency for a continuous airflow containing 1 ppm O₃ over a wide humidity range (0–80% RH) at room temperature. Under the same conditions, the O₃ removal efficiency of PCN-250(Fe₂Co) was higher than those of many representative materials, including α-Fe₂O₃, Co₃O₄, CoFe₂O₄, activated charcoal, and MIL-100(Fe). PCN-250(Fe₂Co) also showed higher catalytic activity for O₃ decomposition than ZZU-281 under dry conditions. The highly porous and crystalline structure of PCN-
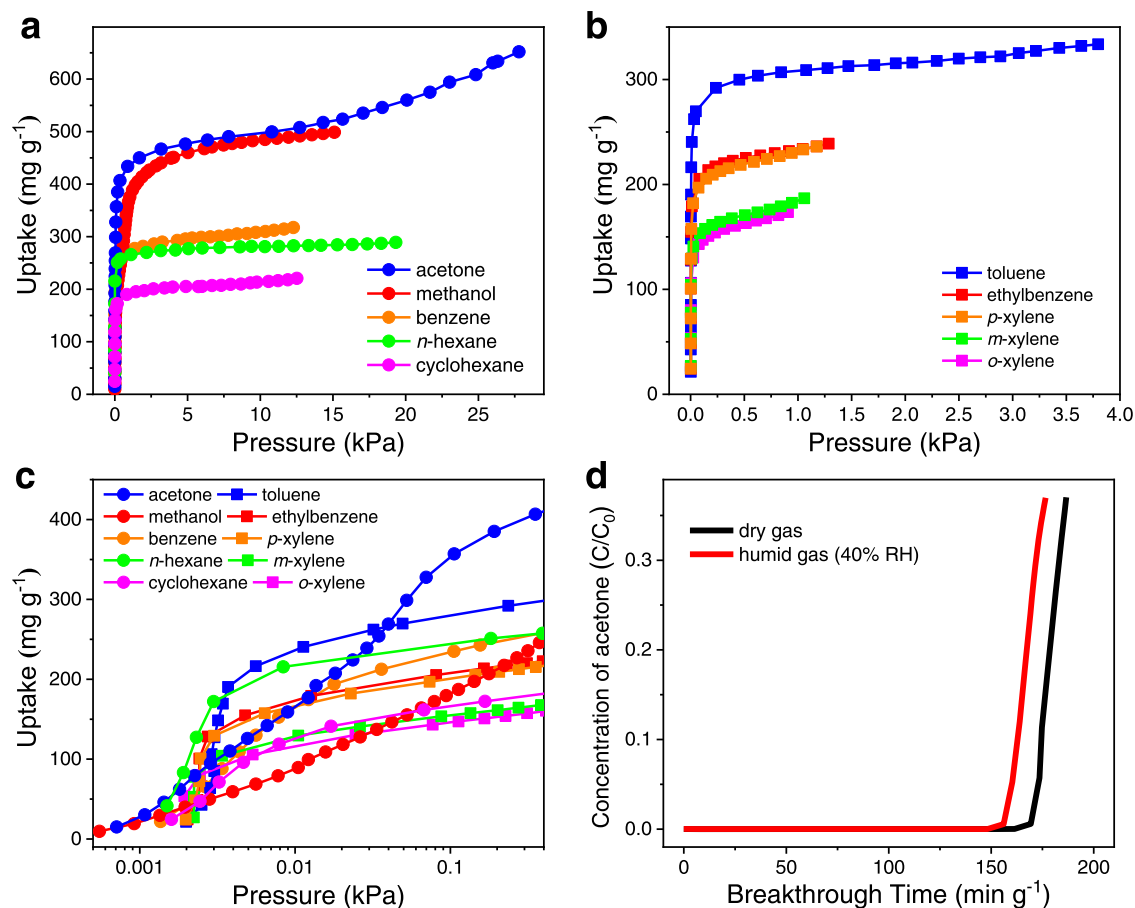
Fig. 5 | VOCs adsorption studies for PCN-250(Fe₂Co). a for relatively low boiling point VOCs (methanol, acetone, benzene, *n*-hexane, and cyclohexane) and **b** for relatively high boiling point VOCs (toluene, ethylbenzene, *o*-xylene, *m*-xylene, and *p*-xylene) recorded at 25 °C. **c** Zoom-in view for adsorption data at the low-pressure range (below 0.4 kPa). **d** Breakthrough curves for dry and humid air (RH = 40% at room temperature) containing acetone vapor (C₀ = 3000 ppm) flowed through a column packed with PCN-250(Fe₂Co). Test conditions: 0.02 g PCN-250(Fe₂Co) diluted with 0.4 g quartz sand, concentration of acetone = 3000 ppm, flow rate = 0.2 L min⁻¹, room temperature.

250(Fe₂Co) remained intact after it was treated by soaking in water for 30 days, or exposing to ambient air for 4 months at room temperature, and its O_3 decomposition capacity retained after exposure of the MOF to relatively high concentration O_3 in dry or humid air (50 ppm). The O_3 decomposition reaction mechanisms catalyzed by PCN-250(Fe₂Co) under dry and wet conditions were proposed based on DFT calculations. It was suggested that the high catalytic performance of PCN-250(Fe₂Co) originated from the introduction of open Co(II) sites as well as its porous structure. Meanwhile, PCN-250(Fe₂Co) is highly potential in the adsorptive removal of VOCs from the air, which is not only a class of hazardous air pollutants but also the precursor of O_3. It is an attribution not available for the other O_3-decomposition catalysts. At a low vapor pressure round 10 Pa and room temperature, PCN-250(Fe₂Co) showed high adsorption capacities (89–241 mg g⁻¹) for ten common VOCs, namely methanol, acetone, *n*-hexane, cyclohexane, benzene, toluene, ethylbenzene, *o*-xylene, *m*-xylene, and *p*-xylene. The VOC capture capacity of PCN-250(Fe₂Co) from both dry and humid air was confirmed by breakthrough experiments. PCN-250(Fe₂Co) may serve as a unique and promising multifunctional material for air purification. This work opens up a new avenue to develop new materials for air pollution control, and the introduction of high porosity to O_3-decomposition catalysts may endow the O_3-decomposition catalysts with multifunctionality, like adsorption, separation, and sensing, which could be beneficial in practical air purification applications.

Methods

Synthesis of PCN-250(Fe₂M) (M = Fe, Co, Ni, Mn)

PCN-250(Fe₂M) was synthesized following the literature with some modifications[40]. Trinuclear complexes [Fe₂M(μ₃-O)(CH₃COO)₆] (M = Fe, Co, Ni, Mn) (45 mg), H₄ABTC (30 mg), and acetic acid (2.0 mL) were ultrasonically dissolved in DMF (6 mL) in a 15 mL high-pressure vessel. The vessel was then tightly sealed, stirred, and heated in an oil bath of 140 °C for 12 h. After cooling down to room temperature, the as-synthesized solid was washed successively with DMF (3 × 40 mL) at 80 °C for 48 h and methanol (3 × 40 mL) at 60 °C for 48 h, and then dried under vacuum at 80 °C for 8 h.

O_3 decomposition measurement

Catalytic O_3 decomposition experiments were conducted with continuous-flow fixed-bed reactors (quartz tube, inner diameter: 4 mm; length: 15 cm) of the tested materials at room temperature (unless otherwise specified) and the inlet gas flow rate of 1 L min⁻¹. Before the test, all tested samples were dried in a vacuum at 80 °C for 12 h. Then a mixture of 30 mg tested materials and 200 mg quartz sand (40–60 mesh) were loaded into the fixed-bed reactors and immobilized by quartz wool. A humidity generator was used to control the humidity of inlet gas. The temperature of the reactor was maintained by a thermostatic water bath. O_3 in the inlet gas was generated by passing zero air through an ultraviolet lamp, and its concentration was controlled by the flow rate of zero air. The O_3 concentration in inlet and outlet gas was detected by an O_3 monitor with a detection limit of

2 ppb. O$_3$ removal efficiency was calculated as $100\% \times (C_{inlet} - C_{outlet})/C_{inlet}$. A schematic representation of the O$_3$ decomposition measurement setup is shown in Supplementary Fig. 14.

Breakthrough experiments

The breakthrough experiments were carried out with zero air containing ca. 3000 ppm acetone vapor by a setup shown in Supplementary Fig. 15. Quartz tubes (4 mm inner diameter and 15 cm length) were packed with a mixture of 20 mg PCN-250(Fe$_2$Co) and 400 mg quartz sand (40–60 mesh). A humidity generator was used to control the humidity of inlet gas (flow rate = 198 mL min^{-1}). The flow rate of air containing saturated acetone vapor at room temperature was controlled by a mass flow controller (Alicat, flow rate = 2 mL min^{-1}). The concentration of acetone in the gases passing through the MOF column was monitored with a Hiden HPR20 mass spectrometer gas analysis system.

Theoretical calculation

A PCN-250(Fe$_2$Co) cluster model is constructed by cutting from its periodic structure as done in recent works[30] (Supplementary Fig. 2a), and it includes the Fe$_2$Co core, six phenyl carboxylic groups coordinated with one Co atom and two Fe atoms, and two water molecules occupying two exposed Fe sites. All calculations presented in this work are performed using the unrestricted density functional theory (DFT) with the hybrid functional PBE0 as implemented in the Gaussian09 package[57–59]. Geometry optimizations are carried out with the LANL2DZ basis sets for the Fe and Co atoms and the 6-31 G* basis sets for the other atoms[60–62]. Dispersion correction is included in geometry optimizations using the empirical formula by Grimme et al.[63]. Frequency calculations are performed at the same level of theory to confirm the nature of stationary points and to obtain zero-point energies (ZPE) and entropy effects. The reported free energies are corrected for dispersion, ZPE, and entropy effects.

Data availability

All data supporting the findings of this study are available within the article and its Supplementary Information, or from the corresponding author upon reasonable request.

References

1. Dickerson, R. R. et al. The impact of aerosols on solar ultraviolet radiation and photochemical smog. *Science* **278**, 827–830 (1997).
2. Paoletti, E., De Marco, A., Beddows, D. C., Harrison, R. M. & Manning, W. J. Ozone levels in European and USA cities are increasing more than at rural sites, while peak values are decreasing. *Environ. Pollut.* **192**, 295–299 (2014).
3. Li, P. et al. Nationwide ground-level ozone measurements in China suggest serious risks to forests. *Environ. Pollut.* **237**, 803–813 (2018).
4. Cooper, O. R., Langford, A. O., Parrish, D. D. & Fahey, D. W. Challenges of a lowered U.S. ozone standard. *Science* **348**, 1096–1097 (2015).
5. Lu, X. et al. Severe surface ozone pollution in China: a global perspective. *Environ. Sci. Technol. Lett.* **5**, 487–494 (2018).
6. Weschler, C. J. Ozone in indoor environments: concentration and chemistry. *Indoor Air* **10**, 269–288 (2000).
7. Chang, L.-T. et al. Indoor ozone levels, houseplants and peak expiratory flow rates among healthy adults in Taipei, Taiwan. *Environ. Int.* **122**, 231–236 (2019).
8. Guo, C., Gao, Z. & Shen, J. Emission rates of indoor ozone emission devices: a literature review. *Build. Environ.* **158**, 302–318 (2019).
9. Hubbell, B. J., Hallberg, A., McCubbin, D. R. & Post, E. Health-related benefits of attaining the 8-hr ozone standard. *Environ. Health Perspect.* **113**, 73–82 (2005).
10. Turner, M. C. et al. Long-term ozone exposure and mortality in a large prospective study. *Am. J. Respir. Crit. Care Med.* **193**, 1134–1142 (2016).
11. WHO. *Air quality guidelines: global update 2005*. (World Health Organization, 2006).
12. Chen, Z. et al. Understanding the causal influence of major meteorological factors on ground ozone concentrations across China. *J. Clean. Prod.* **242**, 118498 (2020).
13. Li, G. et al. Widespread and persistent ozone pollution in eastern China during the non-winter season of 2015: observations and source attributions. *Atmos. Chem. Phys.* **17**, 2759–2774 (2017).
14. Wang, T. et al. Ozone pollution in China: a review of concentrations, meteorological influences, chemical precursors, and effects. *Sci. Total Environ.* **575**, 1582–1596 (2017).
15. Mehandjiev, D. & Naidenov, A. Ozone decomposition on α-Fe$_2$O$_3$ catalyst. *Ozone. Sci. Eng.* **14**, 277–282 (1992).
16. lvarez, P. M. A., Masa, F. J., Jaramillo, J., Beltra´n, F. J. & Go´mez-Serrano, V. Kinetics of ozone decomposition by granular activated carbon. *Ind. Eng. Chem. Res.* **47**, 2545–2553 (2008).
17. Yang, S., Nie, J., Wei, F. & Yang, X. Removal of ozone by carbon nanotubes/quartz fiber film. *Environ. Sci. Technol.* **50**, 9592–95928 (2016).
18. Ma, J., Wang, C. & He, H. Transition metal doped cryptomelane-type manganese oxide catalysts for ozone decomposition. *Appl. Catal. B* **201**, 503–510 (2017).
19. Mathew, T. et al. Mesoporous ferrihydrite-based iron oxide nanoparticles as highly promising materials for ozone removal. *Angew. Chem. Int. Ed.* **123**, 7519–7522 (2011).
20. Zhu, G. et al. Surface oxygen vacancy induced α-MnO$_2$ nanofiber for highly efficient ozone elimination. *Appl. Catal. B* **209**, 729–737 (2017).
21. Cao, R., Li, L. & Zhang, P. Macroporous MnO$_2$-based aerogel crosslinked with cellulose nanofibers for efficient ozone removal under humid condition. *J. Hazard. Mater.* **407**, 124793 (2021).
22. Gong, S. et al. Highly active and humidity resistive perovskite LaFeO$_3$ based catalysts for efficient ozone decomposition. *Appl. Catal. B* **241**, 578–587 (2019).
23. Tang, W.-X., Liu, H.-D., Wu, X.-F. & Chen, Y.-F. Higher oxidation state responsible for ozone decomposition at room temperature over manganese and cobalt oxides: effect of calcination temperature. *Ozone. Sci. Eng.* **36**, 502–512 (2014).
24. Ma, J., Chen, Y., He, G. & He, H. A robust H-transfer redox mechanism determines the high-efficiency catalytic performance of layered double hydroxides. *Appl. Catal. B* **285**, 119806 (2021).
25. Gong, S. et al. Gram-scale synthesis of ultra-fine Cu$_2$O for highly efficient ozone decomposition. *RSC Adv.* **10**, 5212–5219 (2020).
26. Zhou, H.-C., Long, J. R. & Yaghi, O. M. Introduction to metal-organic frameworks. *Chem. Rev.* **112**, 673–674 (2012).
27. Furukawa, H., Cordova, K. E., O'Keeffe, M. & Yaghi, O. M. The chemistry and applications of metal-organic frameworks. *Science* **341**, 1230444 (2013).
28. Lv, X.-L. et al. A base-resistant metalloporphyrin metal-organic framework for C-H bond halogenation. *J. Am. Chem. Soc.* **139**, 211–217 (2017).
29. Al-Attas, T. A. et al. Ligand-engineered metal–organic frameworks for electrochemical reduction of carbon dioxide to carbon monoxide. *ACS Catal.* **11**, 7350–7357 (2021).
30. Wang, H. et al. An iron-containing metal-organic framework as a highly efficient catalyst for ozone decomposition. *Angew. Chem. Int. Ed.* **57**, 16416–16420 (2018).
31. Sun, Z.-B., Si, Y.-N., Zhao, S.-N., Wang, Q.-Y. & Zang, S.-Q. Ozone decomposition by a manganese-organic framework over the entire humidity range. *J. Am. Chem. Soc.* **143**, 5150–5157 (2021).
32. Zhou, D.-D. et al. Intermediate-sized molecular sieving of styrene from larger and smaller analogues. *Nat. Mater.* **18**, 994–998 (2019).

33. Cao, J. W. et al. One-step ethylene production from a four-component gas mixture by a single physisorbent. *Nat. Commun.* **12**, 6507 (2021).

34. Pei, J. et al. Dense packing of acetylene in a stable and low-cost metal–organic framework for efficient C_2H_2/CO_2 Separation. *Angew. Chem. Int. Ed.* **60**, 25068–25074 (2021).

35. Xie, L.-H., Liu, X.-M., He, T. & Li, J.-R. Metal-organic frameworks for the capture of trace aromatic volatile organic compounds. *Chem.* **4**, 1911–1927 (2018).

36. Lai, C. et al. Metal-organic frameworks as burgeoning materials for the capture and sensing of indoor VOCs and radon gases. *Coord. Chem. Rev.* **427**, 213565 (2021).

37. Liu, B. et al. Catalytic ozonation of VOCs at low temperature: a comprehensive review. *J. Hazard. Mater.* **422**, 126847 (2022).

38. Abednatanzi, S. et al. Mixed-metal metal-organic frameworks. *Chem. Soc. Rev.* **48**, 2535–2565 (2019).

39. Chen, L., Wang, H.-F., Li, C. & Xu, Q. Bimetallic metal-organic frameworks and their derivatives. *Chem. Sci.* **11**, 5369–5403 (2020).

40. Feng, D. et al. Kinetically tuned dimensional augmentation as a versatile synthetic route towards robust metal-organic frameworks. *Nat. Commun.* **5**, 5723 (2014).

41. Dhakshinamoorthy, A. et al. Iron(iii) metal–organic frameworks as solid Lewis acids for the isomerization of α-pinene oxide. *Catal. Sci. Technol.* **2**, 324–330 (2012).

42. Cai, C. et al. Efficient degradation of clofibric acid by heterogeneous catalytic ozonation using $CoFe_2O_4$ catalyst in water. *J. Hazard. Mater.* **410**, 124604 (2021).

43. Subrahmanyam, C., Bulushev, D. A. & Kiwi-Minsker, L. Dynamic behaviour of activated carbon catalysts during ozone decomposition at room temperature. *Appl. Catal. B* **61**, 98–106 (2005).

44. Ondarts, M., Outin, J., Reinert, L., Gonze, E. & Duclaux, L. Removal of ozone by activated carbons modified by oxidation treatments. *Eur. Phys. J. Spec. Top.* **224**, 1995–1999 (2015).

45. He, T., Kong, X.-J. & Li, J.-R. Chemically stable metal-organic frameworks: rational construction and application expansion. *Acc. Chem. Res.* **54**, 3083–3094 (2021).

46. Burtch, N. C., Jasuja, H. & Walton, K. S. Water stability and adsorption in metal-organic frameworks. *Chem. Rev.* **114**, 10575–10612 (2014).

47. Lv, X.-L. et al. Ligand rigidification for enhancing the stability of metal-organic frameworks. *J. Am. Chem. Soc.* **141**, 10283–10293 (2019).

48. He, T. et al. Kinetically controlled reticular assembly of a chemically stable mesoporous Ni(II)-pyrazolate metal-organic framework. *J. Am. Chem. Soc.* **142**, 13491–13499 (2020).

49. Yang, H. et al. Ultrastable high-connected chromium metal-organic frameworks. *J. Am. Chem. Soc.* **143**, 14470–14474 (2021).

50. Guillerm, V., Xu, H., Albalad, J., Imaz, I. & Maspoch, D. Postsynthetic selective ligand cleavage by solid-gas phase ozonolysis fuses micropores into mesopores in metal-organic frameworks. *J. Am. Chem. Soc.* **140**, 15022–15030 (2018).

51. Yue, C. et al. Study on the stability, evolution of physicochemical properties, and postsynthesis of metal-organic frameworks in bubbled aqueous ozone solution. *ACS Appl. Mater. Interfaces* **13**, 26264–26277 (2021).

52. Cozzolino, A. F. et al. Ligand redox non-innocence in the stoichiometric oxidation of Mn_2(2,5-dioxidoterephthalate) (Mn-MOF-74). *J. Am. Chem. Soc.* **136**, 3334–3337 (2014).

53. Chen, Y. et al. Unusual moisture-enhanced CO_2 capture within microporous PCN-250 frameworks. *ACS Appl. Mater. Interfaces* **10**, 38638–38647 (2018).

54. Oyama, S. T. Chemical and catalytic properties of ozone. *Catal. Rev.* **42**, 279–322 (2000).

55. Campestrini, S., Robert, A. & Meunier, B. Ozone epoxidation of olefins catalyzed by highly robust manganese and iron porphyrin complexes. *J. Org. Chem.* **56**, 3725–3727 (1991).

56. Sharma, M., Meehan, E., Mercado, B. Q. & Bruckner, C. β-Alkyloxazolochlorins: revisiting the ozonation of octaalkylporphyrins, and beyond. *Chem. Eur. J.* **22**, 11706–11718 (2016).

57. Parr, R. G. & Yang, W. *Density-Functional Theory of Atoms and Molecules*. (Oxford University Press, New York, 1994).

58. Perdew, J. P., Burke, K. & Ernzerhof, M. Generalized gradient approximation made simple. *Phys. Rev. Lett.* **77**, 3865–3868 (1996).

59. Frisch, M. J. et al. *Gaussian 09, Revision A.02*. (Gaussian, Inc., 2009).

60. Hay, P. J. & Wadt, W. R. Ab initio effective core potentials for molecular calculations. Potentials for K to Au including the outermost core orbitals. *J. Chem. Phys.* **82**, 299–310 (1985).

61. Ditchfield, R., Hehre, W. J. & Pople, J. A. Self-consistent molecular-orbital methods. IX. An extended gaussian-type basis for molecular-orbital studies of organic molecules. *J. Chem. Phys.* **54**, 724–728 (1971).

62. Hariharan, P. C. & Pople, J. A. The influence of polarization functions on molecular orbital hydrogenation energies. *Theor. Chem. Acc.* **28**, 213–222 (1973).

63. Grimme, S., Antony, J., Ehrlich, S. & Krieg, H. A consistent and accurate ab initio parametrization of density functional dispersion correction (DFT-D) for the 94 elements H-Pu. *J. Chem. Phys.* **132**, 154104 (2010).

Acknowledgements

Author contributions

J.R.L., L.H.X., and C.D. conceived the project. C.D. and L.H.X. designed the experiments. C.D. prepared and characterized the samples. C.D., L.H.X., and J.R.L analyzed the experimental data and discussed the results. J.J.Y., W.H.F., and G.C. carried out DFT calculations. C.D., J.J.Y., and L.H.X. wrote the manuscript. W.H.F., G.C., and J.R.L. guided and supervised the project. All authors reviewed and contributed to the final manuscript.

Competing interests

The authors declare no competing interests.

Additional information

Supplementary information The online version contains supplementary material available at https://doi.org/10.1038/s41467-022-32678-2.

Correspondence and requests for materials should be addressed to Lin-Hua Xie, Ganglong Cui or Jian-Rong Li.

Peer review information *Nature Communications* thanks the anonymous reviewers for their contribution to the peer review of this work.

Reprints and permission information is available at http://www.nature.com/reprints